# Radium Ion Spectroscopy

Giri, Gouri Shankar

# Chapter 5

# Spectroscopy of Short-Lived Radium Isotopes in an Ion Trap

Precision laser spectroscopy of trapped radium ions in a linear Paul trap provides a new quality to the spectroscopic data which are relevant for the development of an experiment to measure the parity violating weak interaction effects in this system. Here we present and discuss the measurements of hyperfine structures, isotopes shifts, and lifetime, using trapped radium ions in a linear Paul trap. The measurements provide the following results.

- Hyperfine structure intervals of the $6d\ ^2D_{3/2}$ state in $^{209,211,213}Ra^+$.
- Isotope shifts of the $6d\ ^2D_{3/2}$ - $7p\ ^2P_{1/2}$ transition (1079 nm) in $^{209-214}Ra^+$.
- Isotope shifts of the $6d\ ^2D_{3/2}$ - $7p\ ^2P_{3/2}$ transition (708 nm) in $^{212-214}Ra^+$.
- Lifetime of the $6d\ ^2D_{5/2}$ state in $^{212}Ra^+$.

The results provide a benchmark for the required atomic theory, the precision of which is indispensable for the interpretation of results from the planned measurement of parity violation in $Ra^+$.

## 5.1 Hyperfine Structure Interval of $6d\ ^2D_{3/2}$ State

A description of hyperfine structure is given in Appendix B. Elaborate details can be found in atomic physics textbooks [107, 112, 113]. We have measured the hyperfine structure interval of the $6d\ ^2D_{3/2}$ state in three isotopes with $I \neq 0$. The isotopes we have studied are $^{213}Ra^+$ ($I$=1/2) and $^{209,211}Ra^+$ ($I$=5/2). The relevant level schemes are shown in Fig. 5.1.

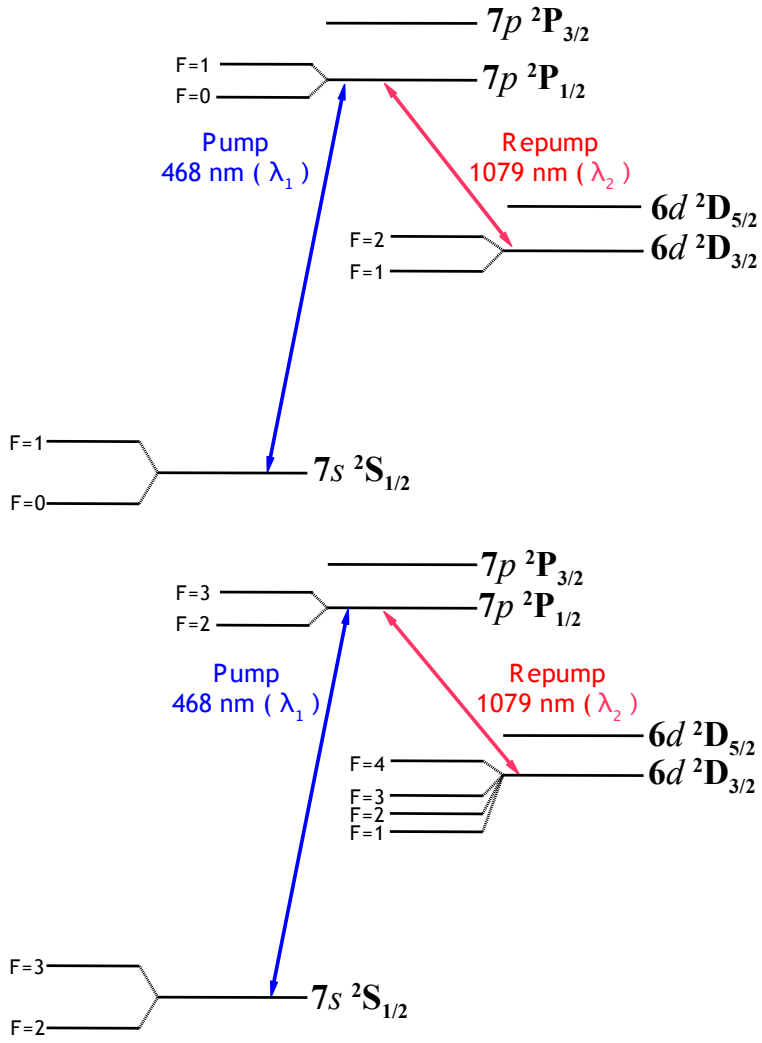


**Fig. 5.1:** Level schemes of odd isotopes with hyperfine structures. Upper and lower figures correspond to $^{213}$Ra$^+$ ($I$=1/2) and $^{209,211}$Ra$^+$ ($I$=5/2) respectively.

To measure the hyperfine structure interval of the $6d\ ^2D_{3/2}$ state in $^{213}$Ra$^+$, frequencies of the light from two pump lasers at wavelengths $\lambda_1$ are tuned to continuously pump each hyperfine level (F=0 and F=1) of the ground $7s\ ^2S_{1/2}$ state, thereby exciting the ions to both hyperfine levels (F=0 and F=1) of the excited $7p\ ^2P_{1/2}$ state. The hyperfine structure interval of the $7s\ ^2S_{1/2}$ state in $^{213}$Ra$^+$ has been determined to be 22920(6) MHz [79]. Hence two lasers are employed to pump the ground state hyperfine levels. From the excited $7p\ ^2P_{1/2}$ hyperfine levels, the ions decay to the metastable $6d\ ^2D_{3/2}$ hyperfine levels (F=1 and F=2). Light from a repump laser at wavelength $\lambda_2$ is scanned over the $6d\ ^2D_{3/2}$(F=1, 2) - $7p\ ^2P_{1/2}$(F=0, 1) resonances. Many such scans are averaged to obtain a good

signal-to-noise ratio. Data are collected for a few hours to accumulate enough statistics. The observed resonances are shown in Fig. 5.2.

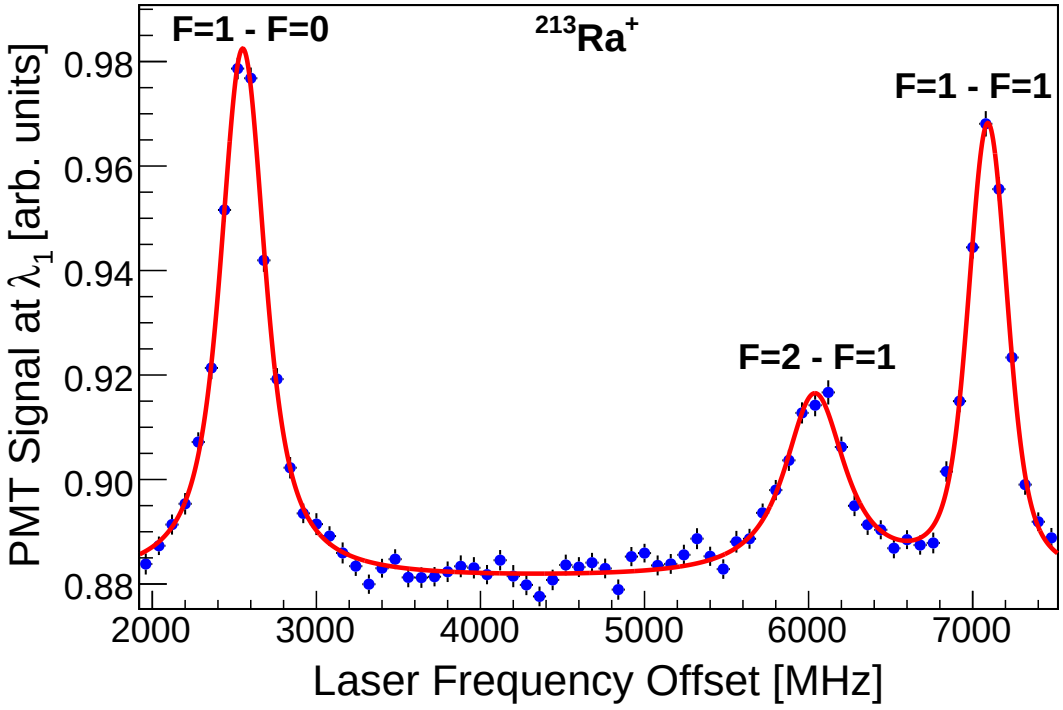


**Fig. 5.2:** Hyperfine structure intervals of $6d\ ^2D_{3/2}$ and $7p\ ^2P_{1/2}$ states in $^{213}Ra^+$. The solid line represents a fit of three Voigt profiles to the data. The Gaussian widths of the transitions are 181(20) MHz (FWHM).

For this measurement nitrogen ($N_2$) is used as a buffer gas at $3 \times 10^{-3}$ mbar. This results in hyperfine mixing of the $6d\ ^2D_{3/2}$ hyperfine levels. This effect prevents any possible shelving of ions to the metastable $6d\ ^2D_{3/2}$ F=1 or F=2 state while the $6d\ ^2D_{3/2}$ F=2 or F=1 state is depopulated by the resonant light at wavelength $\lambda_2$. The frequency is calibrated with an infrared wavelength meter. The measured hyperfine structure interval of 4542(7) MHz for the $7p\ ^2P_{1/2}$ state is within 2 standard deviations off the value 4525(5) MHz as measured at ISOLDE [79]. The hyperfine structure interval for the $6d\ ^2D_{3/2}$ state is measured as 1055(10) MHz. The hyperfine structure constants $A$ for the $6d\ ^2D_{3/2}$ and $7p\ ^2P_{1/2}$ states are listed in Table 5.1. The theoretical values [26,84] quoted in Table 5.1 are calculated for $^{213}Ra^+$ by scaling with $I/I' \times \mu_I'/\mu_I$. The relevant nuclear magnetic moments ($\mu_I$) and the electric quadrupole moments are taken from [81, 83].

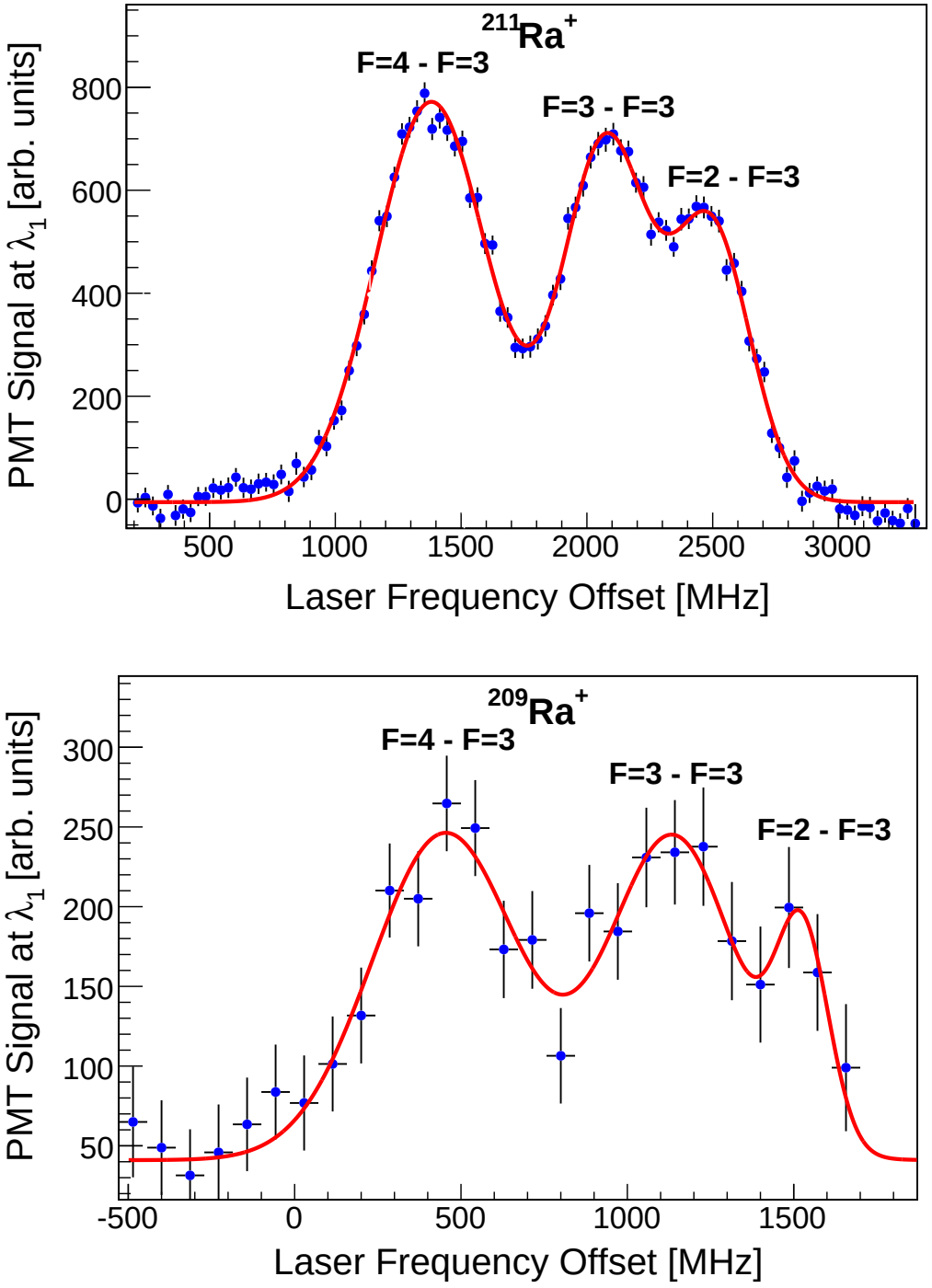


**Fig. 5.3:** Hyperfine structure intervals of the $6d\ ^2D_{3/2}$ states in $^{209,211}Ra^+$. $6d\ ^2D_{3/2}$(F=2,3,4) - $7p\ ^2P_{1/2}$(F=3) transitions are shown. The solid line in each case represents a fit of three Gaussian functions to the data. The top and bottom figures correspond to $^{211}Ra^+$ and $^{209}Ra^+$ respectively.

To measure the hyperfine structure intervals of the $6d\ ^2D_{3/2}$ states in $^{209,211}Ra^+$, frequencies of the light from two pump lasers at wavelengths $\lambda_1$ are tuned to continuously pump both hyperfine levels (F=2 and F=3) of the ground $7s\ ^2S_{1/2}$ state for the isotope under investigation. The hyperfine structure interval of the $7s\ ^2S_{1/2}$ state in $^{211}Ra^+$ has been determined to be 19874.4(3.0) MHz [79]. Though there is no reported value for $^{209}Ra^+$, it is expected to be comparable to that of $^{211}Ra^+$ due to the fact that the two isotopes have comparable mass and identical nuclear spin. The two pump lasers excite the ions to the hyperfine level F=3 of the excited $7p\ ^2P_{1/2}$ state from which the ions decay to the three out of the four metastable $6d\ ^2D_{3/2}$ hyperfine levels (F=2, 3, 4). This pumping scheme ensures that ions do not decay to the $6d\ ^2D_{3/2}$(F=1) state. Light from a repump laser at wavelength $\lambda_2$ is scanned over the $6d\ ^2D_{3/2}$(F=2, 3, 4) - $7p\ ^2P_{1/2}$(F=3) resonances of the isotope under investigation. Many such scans are averaged to obtain a good signal-to-noise ratio. Data were collected for a few hours to accumulate enough statistics and to resolve the lines. The observed resonances are shown in Fig. 5.3. In case of $^{209}Ra^+$, the signal-to-noise ratio is very low. This is a consequence of very low production yield and shorter lifetime of this particle as discussed in section 4.1.5.

For these measurements neon (Ne) is used as a buffer gas. To ensure collision induced hyperfine mixing of the $6d\ ^2D_{3/2}$ hyperfine levels, a higher buffer gas pressure ($1 \times 10^{-2}$ mbar) is used, which is different from the measurements in $^{213}Ra^+$. This effect prevents any possible shelving of ions to the metastable $6d\ ^2D_{3/2}$ hyperfine levels while the $6d\ ^2D_{3/2}$ state is depopulated by the resonant light at wavelength $\lambda_2$. The frequency is calibrated with a reference laser which is referenced to an optical frequency comb. The hyperfine structure constants $A$ and $B$ for the $6d\ ^2D_{3/2}$ state are listed in Table 5.2. The theoretical values [75]

**Table 5.1:** Hyperfine structure constants $A(6d\ ^2D_{3/2})$ and $A(7p\ ^2P_{1/2})$ for $^{213}Ra^+$. The most recent theoretical values are scaled for $^{213}Ra^+$ using $I/I' \times \mu_I'/\mu_I$ with the experimentally measured magnetic moments [83].

| | $A(6d\ ^2D_{3/2})$ MHz | $A(7p\ ^2P_{1/2})$ MHz |
|---|---|---|
| This work | 528(5) | 4542(7) |
| ISOLDE [79] | - | 4525(5) |
| Theory [26] | 543 | 4555 |
| Theory [84] | 541 | 4565 |

**Table 5.2:** Hyperfine structure constants $A(6d\ ^2D_{3/2})$ and $B(6d\ ^2D_{3/2})$ for $^{209,211}Ra^+$.

| Isotope | $A(6d\ ^2D_{3/2})$ MHz | $B(6d\ ^2D_{3/2})$ MHz |
|---|---|---|
| $^{211}Ra^+$ | 151(2) | 103(6) |
| | 150* | 147* |
| $^{209}Ra^+$ | 148(10) | 104(38) |
| | 148* | 122* |

*The most recent theoretical values [75] are scaled for $^{209,211}Ra^+$ using the experimentally measured magnetic and quadrupole moments [81, 83].

quoted in Table 5.2 are calculated for $^{209,211}Ra^+$ by scaling with $I/I' \times \mu_I'/\mu_I$ for the hyperfine constant $A$ and with $I/I' \times Q_I'/Q_I$ for the hyperfine constant $B$. The relevant nuclear magnetic moments ($\mu_I$) and the electric quadrupole moments ($Q_I$) are taken from [81, 83].

To summarize, we have measured the hyperfine structure intervals of the $6d\ ^2D_{3/2}$ states in three isotopes with $I \neq 0$. They are listed in Table 5.3. The $6d\ ^2D_{3/2}$ state is of particular importance for the $7s\ ^2S_{1/2}$ - $6d\ ^2D_{3/2}$ transition relevant for the planned APV measurement in $Ra^+$. The measured hyperfine structure intervals and the corresponding hyperfine constants $A$ and $B$ as listed in Table 5.1 and 5.2 are an important probe of the atomic wavefunction in $Ra^+$.

**Table 5.3:** Hyperfine structure intervals between the hyperfine levels F and F-1 for the $6d\ ^2D_{3/2}$ state in $^{209,211,213}Ra^+$.

| | $211Ra^+(I=5/2)$ | $209Ra^+(I=5/2)$ | $213Ra^+(I=1/2)$ |
|---|---|---|---|
| F | $\Delta$E MHz | $\Delta$E MHz | $\Delta$E MHz |
| 4 | 686(9) | 673(28) | - |
| 3 | 407(7) | 396(49) | - |
| 2 | - | - | 1055(10) |

## 5.2 Isotope Shifts

A description of isotope shifts is given in Appendix C. Elaborate details can be found in atomic physics textbooks [107, 112, 113]. We have measured isotope

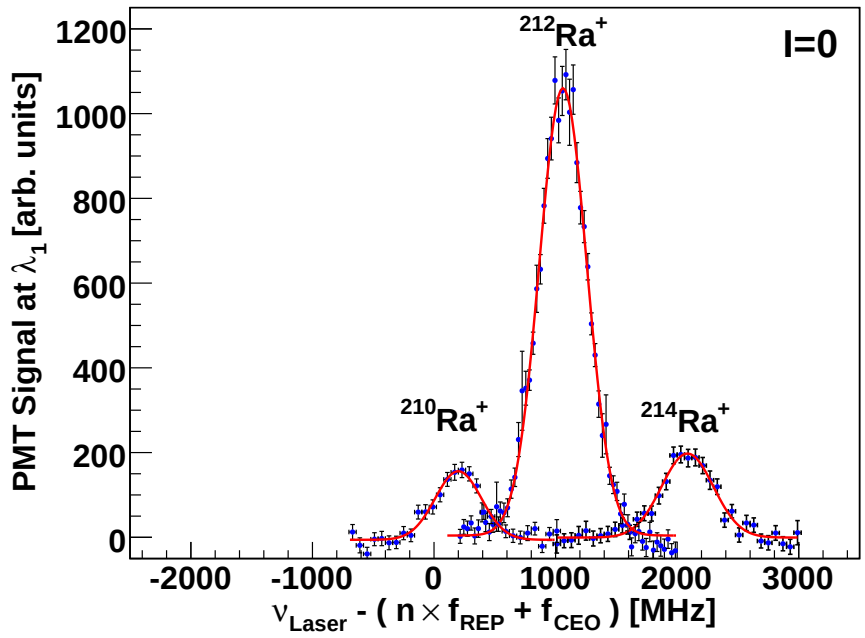


**Fig. 5.4:** Isotope shift of $6d\ ^2D_{3/2}$ - $7p\ ^2P_{1/2}$ transition in $^{210,212,214}Ra^+$. The solid line represents in each case a fit of a Gaussian function to the data.

shifts of the $6d\ ^2D_{3/2}$ - $7p\ ^2P_{1/2}$ tansition in six isotopes and shifts of the $6d\ ^2D_{3/2}$ - $7p\ ^2P_{3/2}$ tansition in three isotopes.

### 5.2.1 Isotope Shifts of $6d\ ^2D_{3/2}$ - $7p\ ^2P_{1/2}$ Transition

Isotope shifts have been measured for the $6d\ ^2D_{3/2}$ - $7p\ ^2P_{1/2}$ transition in $^{209-214}Ra^+$. Determination of isotope shifts for a transition in a range of isotopes requires knowledge of the frequencies of the transition for all the concerned isotopes relative to a common frequency reference. For the results reported here, a frequency comb serves as the reference to which relative differences in the frequencies are determined.

For the isotopes with $I$=0 ($^{210,212,214}Ra^+$) the frequencies of the $6d\ ^2D_{3/2}$ - $7p\ ^2P_{1/2}$ transition are determined with light from one laser at wavelength $\lambda_1$ which continuously pumps the ground $7s\ ^2S_{1/2}$ state to the excited $7p\ ^2P_{1/2}$ state from which the ions decay to the $6d\ ^2D_{3/2}$ state with about 10% branching ratio. Light from another laser at wavelength $\lambda_2$ is scanned over the resonance of $6d\ ^2D_{3/2}$ - $7p\ ^2P_{1/2}$ transition. The observed resonances are shown in Fig. 5.4.

The principle of measurement as described for the measurement of hyper-

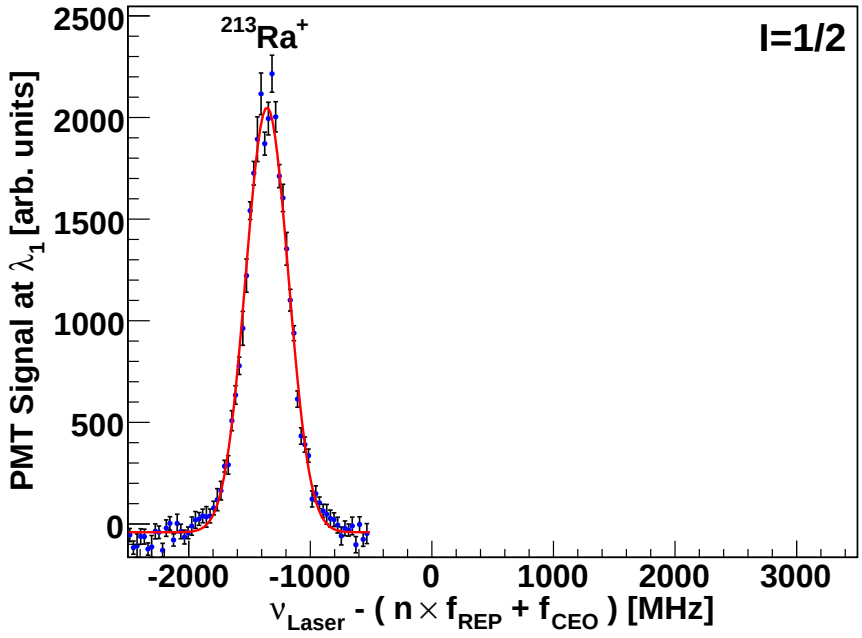


**Fig. 5.5:** Isotope shift of $6d\ ^2D_{3/2}$ - $7p\ ^2P_{1/2}$ transition in $^{213}Ra^+$. $6d\ ^2D_{3/2}$(F=0)-$7p\ ^2P_{1/2}$(F=1) transition is shown. The solid line represents a fit of a Gaussian function to the data.

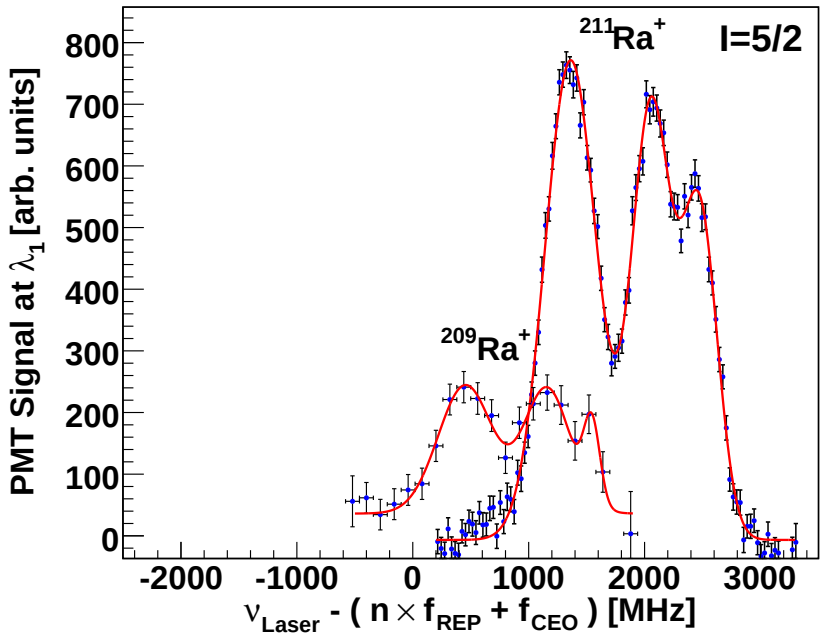


**Fig. 5.6:** Isotope shift of $6d\ ^2D_{3/2}$ - $7p\ ^2P_{1/2}$ transition in $^{209,211}Ra^+$. $6d\ ^2D_{3/2}$(F=2, 3, 4) - $7p\ ^2P_{1/2}$(F=3) transitions are shown, where the peaks at the lowest frequency in each case correspond to the $6d\ ^2D_{3/2}$(F=4) - $7p\ ^2P_{1/2}$(F=3) transition. The solid line represents in each case a fit of three Gaussian functions to the data.

fine structure applies for the isotopes with $I \neq 0$ ($^{209,211,213}Ra^{+}$). The measured transitions are shown in Figs. 5.5 and 5.6.

For the measurement of isotopes shifts only neon is used in order to minimize the influence of buffer gas on the resonance line shapes. As shown in Figs. 5.4-5.6 all the measured transitions have been calibrated to a common frequency axis where the offset frequency of the laser has been given relative to the $n$=1111032 comb line which has an absolute frequency of 277,803,572.31(3) MHz. The principle of absolute calibration for the $6d\ ^2D_{3/2}$ - $7p\ ^2P_{1/2}$ transition has been given section 4.4.1.

### 5.2.2 Isotope Shifts of $6d\ ^2D_{3/2}$ - $7p\ ^2P_{3/2}$ Transition

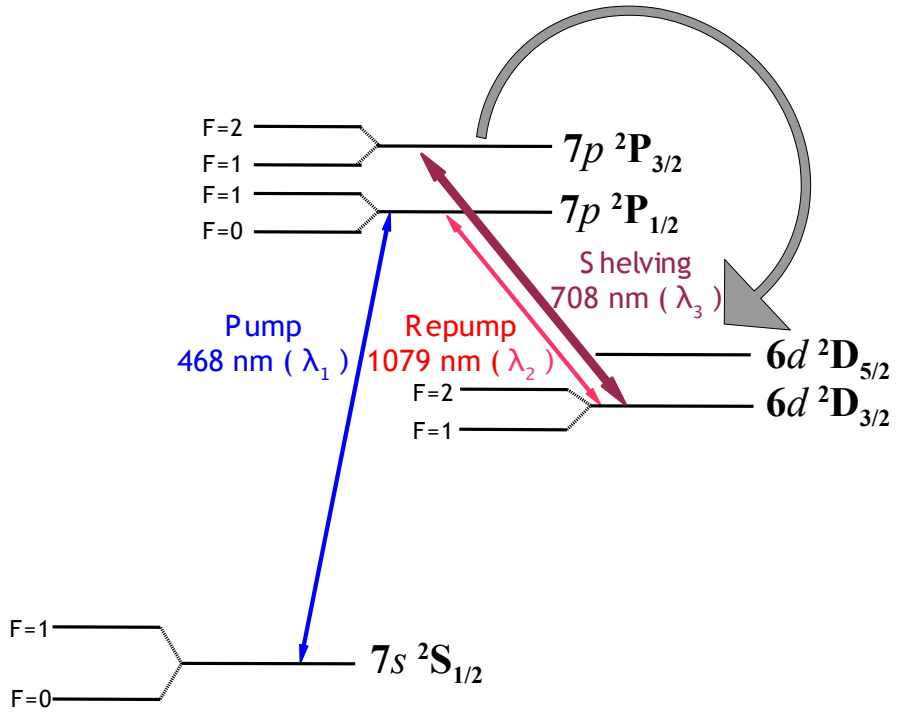


**Fig. 5.7:** Level scheme of $^{213}Ra^{+}$ showing the $6d\ ^2D_{3/2}$ - $7p\ ^2P_{3/2}$ shelving transition.

Isotope shifts have been measured for the $6d\ ^2D_{3/2}$ - $7p\ ^2P_{3/2}$ transition in $^{212,213,214}Ra^{+}$. For this measurement a third laser at wavelength $\lambda_3$=708 nm is employed in addition to the pump and repump lasers as described in the previous measurements. The relevant level scheme is shown in Fig. 5.7.

To determine the isotope shifts of the $6d\ ^2D_{3/2}$ - $7p\ ^2P_{3/2}$ transition, the lasers

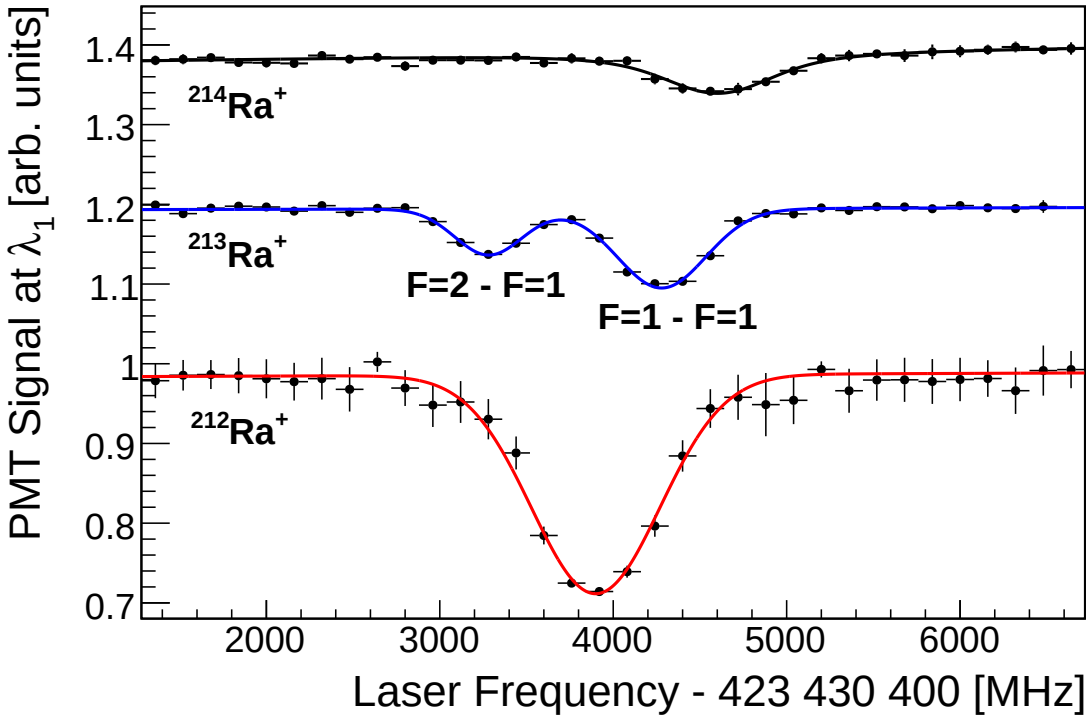


**Fig. 5.8:** Isotope shifts of $6d\ ^2D_{3/2}$ - $7p\ ^2P_{3/2}$ transition in $^{212,213,214}Ra^+$. The solid lines represent in each case a fit of a Voigt profile to the data. The different Gaussian widths are due to different buffer gas pressures at which the measurements are carried out.

operating at wavelengths $\lambda_1$ and $\lambda_2$ are tuned to frequencies corresponding to the resonances for the $7s\ ^2S_{1/2}$ - $7p\ ^2P_{1/2}$ transition and $6d\ ^2D_{3/2}$ - $7p\ ^2P_{1/2}$ transition respectively, for the isotope under investigation. This creates a fluorescence cycle. The frequency of the laser light at $\lambda_3$ is scanned over the $6d\ ^2D_{3/2}$ - $7p\ ^2P_{3/2}$ resonance. Near resonance the ions are pumped from the $6d\ ^2D_{3/2}$ state to the $7p\ ^2P_{3/2}$ state, from which about 10% of the ions decay to the $6d\ ^2D_{5/2}$ state. This is a metastable state where the ions are shelved and they no longer remain in the fluorescence cycle. This creates a dip in the fluorescence signal. This is also known as dark resonance.

By pumping on the $7s\ ^2S_{1/2}$(F=1) - $7p\ ^2P_{1/2}$(F=0) transition and repumping on the $6d\ ^2D_{3/2}$(F=1) - $7p\ ^2P_{1/2}$(F=0) transition, the fluorescence cycle is established for $^{213}Ra^+$. This leaves the $6d\ ^2D_{3/2}$(F=2) state largely depopulated. The $6d\ ^2D_{3/2}$(F=1) - $7p\ ^2P_{3/2}$(F=1) resonance is deformed by the close lying $6d\ ^2D_{3/2}$(F=2) - $7p\ ^2P_{3/2}$(F=2) resonance. The $6d\ ^2D_{3/2}$(F=2) - $7p\ ^2P_{3/2}$(F=1)

resonance has been used to determine the isotope shift of $^{213}Ra^{+}$.

The transitions observed are shown in Fig. 5.8. These measurements have been performed at different gas pressures $3 \times 10^{-3}$, $2 \times 10^{-3}$, $2 \times 10^{-2}$ mbar with neon as the buffer gas.

### 5.2.3 Data Analysis and Results

The isotope shifts of a spectral line are usually parameterized as [114],

$$\delta\nu_{MM'} = (K_{\mathrm{NMS}} + K_{\mathrm{SMS}})\frac{M - M'}{MM'} + F_{\mathrm{FS}}\delta\langle r^2\rangle_{MM'} \tag{5.1}$$

where $\delta\nu_{MM'} = \nu_M - \nu_{M'}$. M and M$'$ are the masses of the reference isotope and the isotope of interest respectively, both in atomic mass units. $K_{\mathrm{NMS}}$ and $K_{\mathrm{SMS}}$ are the normal and specific mass shift components and $F_{\mathrm{FS}}$ is the field shift component. $\delta\langle r^2\rangle_{MM'}$ is the difference in mean square nuclear charge radii, which is common to all transitions for a pair of nuclei. Both the specific mass shift and the field shift are characteristic to a particular transition. Here they are defined as the shift of the lower level, minus the shift of the upper level. The normal mass shift can be calculated from the expression $K_{\mathrm{NMS}} = \nu m_e$, where $\nu$ is the transition frequency and $m_e$ is the mass of electron in atomic mass units.

A King plot analysis [115] is used to separate the specific mass shift and the field shift components. Here the transformed isotope shifts ($\Delta\nu^{\mathrm{King}}_{MM'}$) are taken, which are obtained by subtracting the normal mass shift component from the experimentally measured isotope shifts and multiplying both sides of Eq. (5.1) by $MM'/(M - M')$. Eq. (5.1) is rewritten as

$$\Delta\nu^{\mathrm{King}}_{MM'} = K_{\mathrm{SMS}} + F_{\mathrm{FS}}\ \delta\langle r^2\rangle_{MM'}\frac{MM'}{M - M'} \tag{5.2a}$$

$$= \delta\nu_{MM'}\frac{MM'}{M - M'} - K_{\mathrm{NMS}}. \tag{5.2b}$$

In a comparison between two different optical transitions $i$ and $j$, the transformed isotope shifts can be written as

$$\Delta\nu^{j,\mathrm{King}}_{MM'} = \frac{F^j_{FS}}{F^i_{FS}}\Delta\nu^{i,\mathrm{King}}_{MM'} + K^j_{SMS} - \frac{F^j_{FS}}{F^i_{FS}}K^i_{SMS}. \tag{5.3}$$

This is essentially a linear relation of the transformed isotope shifts of one transition ($\Delta\nu^{j,\mathrm{King}}_{MM'}$) against the corresponding shifts of the other transition ($\Delta\nu^{i,\mathrm{King}}_{MM'}$). The slope yields the ratio of field shifts and the difference in specific mass shifts appears as the crossing with the abscissa.

**Table 5.4:** Isotope shifts of $6d\ ^2D_{3/2}$ - $7p\ ^2P_{1/2}$ transition in $^{209-214}Ra^+$ with the relevant hyperfine constants. The comparatively large error bar on the isotope shift of $^{209}Ra^+$ is a consequence of low signal-to-noise ratio due to lower yield and shorter life time of the isotope. $\delta\nu_{214,M'}$ is the shift of the $6d\ ^2D_{3/2}$ - $7p\ ^2P_{1/2}$ transition with respect to $^{214}Ra^+$.

| Mass Number | $A(6d\ ^2D_{3/2})$ MHz | $B(6d\ ^2D_{3/2})$ MHz | $A(7p\ ^2P_{1/2})$ MHz | $\delta\nu_{214,M'}$ MHz |
|---|---|---|---|---|
| 214 | - | - | - | 0 |
| 213 | 528(5) | - | 4525(5) [79] | 707(14) |
| 212 | - | - | - | 1025(12) |
| 211 | 151(2) | 103(6) | 1299.7(0.8) [79] | 1755(14) |
| 210 | - | - | - | 1884(16) |
| 209 | 148(10) | 104(38) | 1276(20)[a] | 2645(56) |

[a]Calculated using Eq. 5.4.

$^{214}Ra^+$ has been chosen as the reference isotope in order to be consistent with previous work [79]. The difference in transition frequencies for the even isotopes yields directly the isotope shift. For $^{209,211,213}Ra^+(I{\neq}0)$ the isotope shifts are given between the centers of gravity of the $6d\ ^2D_{3/2}$ and $7p\ ^2P_{1/2}$ states. This requires the magnetic dipole $A$ and the electric quadrupole $B$ hyperfine constants for those states (Table 5.4). For the $6d\ ^2D_{3/2}$ state, the hyperfine constants have been derived from measured hyperfine intervals. The hyperfine constants $A$ for the $7p\ ^2P_{1/2}$ state are taken from [79]. For the case of $^{209}Ra^+$ no value has been reported. It is derived with the nuclear magnetic moments $\mu$ [83] using

$$\frac{A(7p\,^2P_{1/2},{}^{209}\,\mathrm{Ra}^+)}{A(7p\,^2P_{1/2},{}^{213}\,\mathrm{Ra}^+)} = \frac{I(^{213}\mathrm{Ra}^+)}{I(^{209}\mathrm{Ra}^+)} \times \frac{\mu(^{209}\mathrm{Ra}^+)}{\mu(^{213}\mathrm{Ra}^+)}. \tag{5.4}$$

The measured isotope shifts for all the even and odd isotopes ($^{209-214}Ra^+$) and the relevant hyperfine constants for the $6d\ ^2D_{3/2}$ and $7p\ ^2P_{1/2}$ states in case of isotopes with $I{\neq}0$ are given in Table 5.4.

A King plot of the transformed isotope shifts of the measured $6d\ ^2D_{3/2}$ - $7p\ ^2P_{1/2}$ transition against the corresponding shifts of the $7s\ ^1S_0$ - $7s7p\ ^1P_1$ transition in neutral radium [79] is shown in Fig. 5.9. The values for the atomic masses of the isotopes are taken from [116]. The normal mass shift coefficient of the $6d\ ^2D_{3/2}$ - $7p\ ^2P_{1/2}$ transition in ionic radium is $K_{\mathrm{NMS}} = 152.4$ GHz amu. For the $7s\ ^1S_0$ - $7s7p\ ^1P_1$ transition in neutral radium, the normal mass shift coeffi-

**Table 5.5:** Isotope shifts of $6d\ ^2D_{3/2}$ - $7p\ ^2P_{3/2}$ transition in $^{212-214}Ra^+$. All values are in MHz. $\delta\nu_{214,M'}$ is the isotope shift of the $6d\ ^2D_{3/2}$ - $7p\ ^2P_{3/2}$ transition with respect to $^{214}Ra^+$.

| Mass Number | $\delta\nu_{214,M'}$ MHz |
|---|---|
| 214 | 0 |
| 213 | 453(34) |
| 212 | 701(50) |

cient is $K_{\mathrm{NMS}} = 340.8$ GHz amu. Plotting the transformed isotope shifts against each other shows that the data satisfies a linear relation within the measurement uncertainties (Fig. 5.9). The slope determines the ratio of field shift coefficients, $F_{FS}^{1079\ \mathrm{nm}}/F_{FS}^{482\ \mathrm{nm}} = -0.342(15)$. The abscissa determines the difference of the specific mass shift to be $-1.9(1.1)$ THz amu.

The frequency of the measured $6d\ ^2D_{3/2}$ - $7p\ ^2P_{3/2}$ resonances are calibrated against the P(146)(2-8) single pass absorption resonance in molecular iodine ($I_2$) at $\nu_{\mathrm{Iodine}}$=423,433,720 MHz [108]. The frequencies of the $6d\ ^2D_{3/2}$ - $7p\ ^2P_{3/2}$ transitions relative to the molecular iodine reference line, $\nu_{\mathrm{Ra^+}}$ - $\nu_{\mathrm{Iodine}}$, are found to be +568(42) MHz, -64(13) MHz, and +1269(23) MHz for $^{212}Ra^+$, $^{213}Ra^+$, and $^{214}Ra^+$ respectively. The linearity of the scan of the laser has been verified with a cavity of finesse 1200 and free spectral range (FSR) 10 GHz. The measured isotope shifts are listed in Table 5.5.

The isotope shifts of the $6d\ ^2D_{3/2}$ - $7p\ ^2P_{3/2}$ transition are measured with reference to $^{214}Ra^+$. For $^{213}Ra^+$, the determination of isotope shift requires knowledge of the hyperfine constant $A$ for the $7p\ ^2P_{3/2}$ state which is not reported. Hence it is extracted using the measured values for the $6d\ ^2D_{3/2}$ state and the values reported in [79,81,83]. A King plot of the $6d\ ^2D_{3/2}$ - $7p\ ^2P_{3/2}$ transition (708 nm) against the $6d\ ^2D_{3/2}$ - $7p\ ^2P_{1/2}$ transition (1079 nm) in $Ra^+$ is shown in Fig. 5.10.

To summarize, we have measured the isotope shifts of $6d\ ^2D_{3/2}$ - $7p\ ^2P_{1/2}$ transition in $^{209-214}Ra^+$ and the shifts of $6d\ ^2D_{3/2}$ - $7p\ ^2P_{3/2}$ transition in $^{212-214}Ra^+$. The isotope shifts of the transitions from the metastable $6d\ ^2D_{3/2}$ state are of particular importance beacause they are sensitive to the short range part of the atomic wavefunctions. The measured isotope shifts are listed in Table 5.4 and 5.5 respectively. They are an important probe of the atomic wavefunctions and the nuclear shape and size.

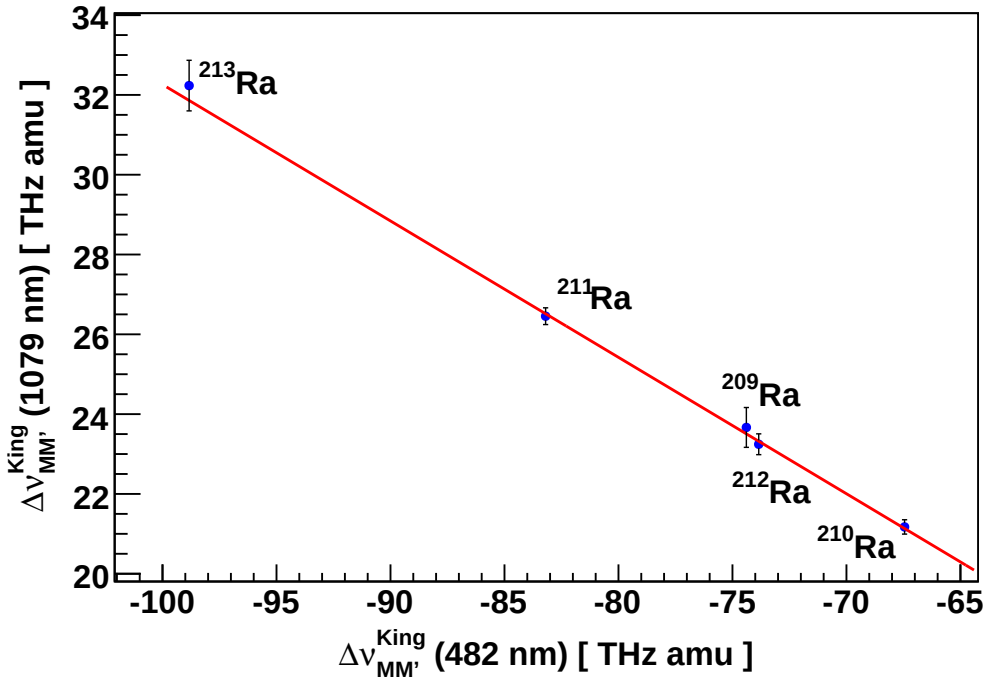


**Fig. 5.9:** King plot of the isotope shift of $6d\ ^2D_{3/2}$ - $7p\ ^2P_{1/2}$ transition at $\lambda$=1079 nm in $Ra^+$ against the corresponding shift of $7s\ ^1S_0$ - $7s7p\ ^1P_1$ transition at $\lambda$=482 nm in the Ra atom. The uncertainties at 482 nm are too small to be visible against the marker size.

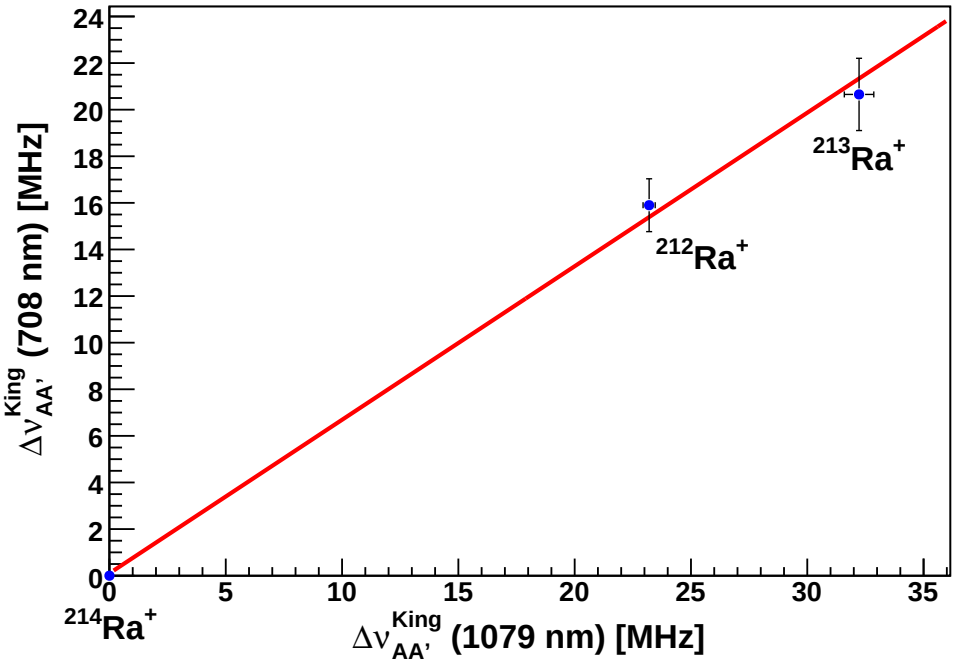


**Fig. 5.10:** A King plot of the isotope shift of $6d\ ^2D_{3/2}$ - $7p\ ^2P_{3/2}$ transition at $\lambda$=708 nm in $Ra^+$ against the corresponding shifts in $\lambda$=1079 nm line in $Ra^+$.

## 5.3 Lifetime of Metastable $6d\ ^2D_{5/2}$ State

The demonstrated shelving of ions from the fluorescence cycle to the $6d\ ^2D_{5/2}$ state by accessing the $6d\ ^2D_{3/2}$ - $7p\ ^2P_{3/2}$ transition as described in section 5.2.2 also enables a measurement of the lifetime of this metastable state [117]. This has been studied only in $^{212}Ra^+$. The lasers at $\lambda_1$, $\lambda_2$, and $\lambda_3$ are tuned to be on resonance for the relevant transitions. The laser at $\lambda_3$ is pulsed with a mechanical chopper wheel with 170 ms on-periods and 670 ms off-periods. When the laser at $\lambda_3$ is on, the $6d\ ^2D_{5/2}$ state is populated via the $7p\ ^2P_{3/2}$ state. When the laser at $\lambda_3$ is off, the $6d\ ^2D_{5/2}$ state gets depopulated and the ions reenter the fluorescence cycle with a time constant equal to the lifetime of the $6d\ ^2D_{5/2}$ state.

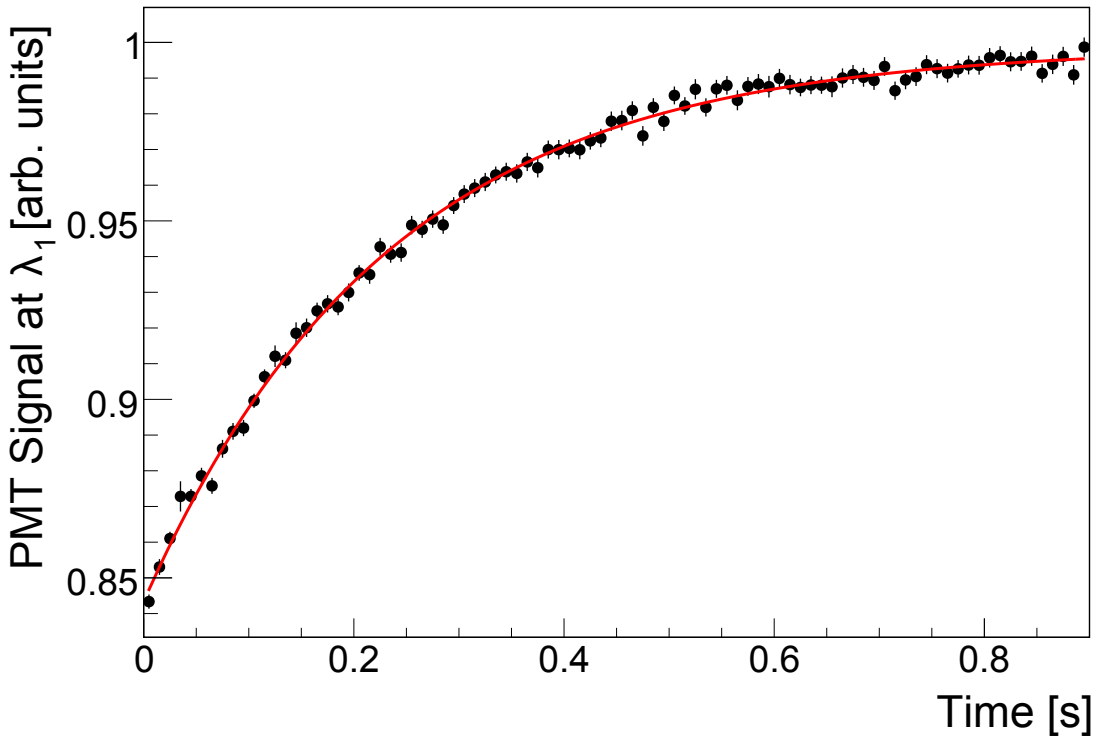


**Fig. 5.11:** Lifetime of $6d\ ^2D_{5/2}$ state in $^{212}Ra^+$ at neon buffer gas pressure $4 \times 10^{-5}$ mbar. The solid line represents a fit of an exponential function to the data.

This is shown in Fig. 5.11. However, the neon buffer gas causes a reduction of the lifetime of the metastable state by quenching it to the ground state. To estimate this effect of the buffer gas, the measurement has been carried out at different gas pressures ranging from $10^{-2}$ to $10^{-5}$ mbar and the lifetime is extrapolated to zero pressure. This is shown in Fig. 5.12. The buffer gas is found to have a

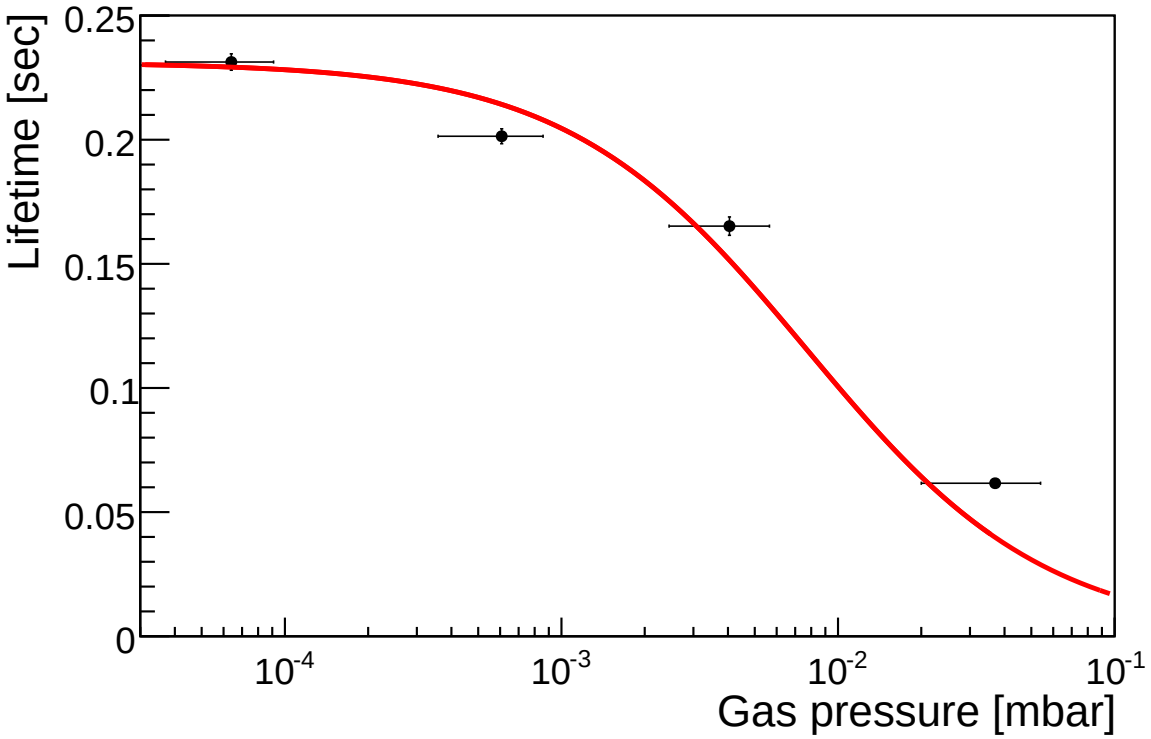


**Fig. 5.12:** Lifetime of $6d\ ^2D_{5/2}$ state in $^{212}Ra^+$ measured at different gas pressures.

strong influence on the radiative lifetime.

Since no detailed theory is currently available to explain the extrapolation to zero pressures, extrapolated radiative life time of 232(4) ms is treated as a lower bound. This number corresponds to the lifetime measured at the lowest pressure of about $4 \times 10^{-5}$ mbar. The theoretical predictions of the radiative lifetime of the metastable $6d\ ^2D_{5/2}$ state in $^{212}Ra^+$ are 297(4) ms [75] and 303(4) ms [84]. Our experimental result confirms that the $6d\ ^2D_{5/2}$ state is long-lived. This is an essential property in view of the long coherence times needed in a single ion APV experiment. The measured lifetimes are important probes of the E2 matrix element which is essential for the APV experiment.

## 5.4 Conclusion

Towards a planned measurement of parity violation in a single trapped ion an experimental set up has been developed within the TRI$\mu$P research program which enables the production and thermalization of radium isotopes. Precision spectroscopy of trapped radium ions in a linear Paul trap yields results on hyperfine

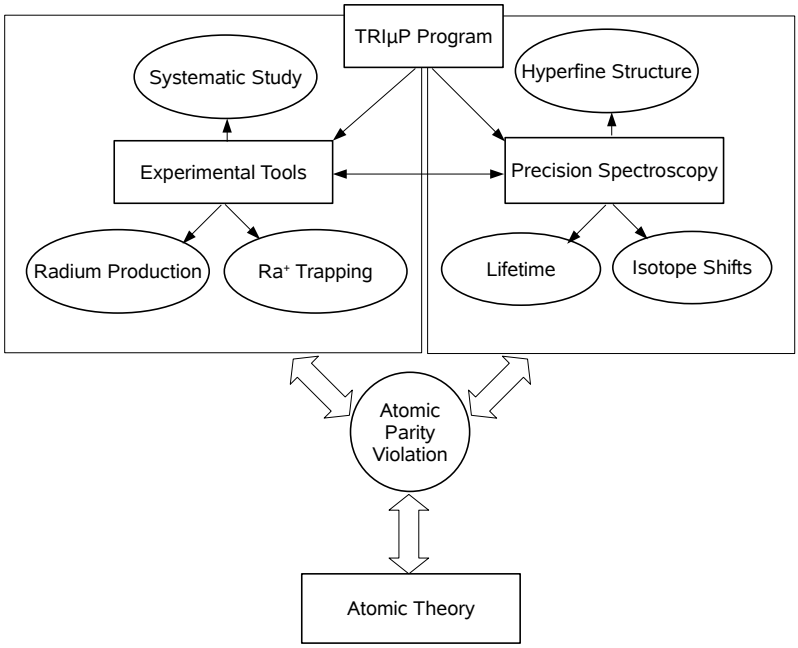


structure intervals, isotope shifts, and lifetime. They are important experimental input for improving the atomic structure calculations.